Exploring a better turbine layout in vertically staggered wind farms

IOP Conf. Series: Journal of Physics: Conf. Series **1037** (2018) 072041 doi:10.1088/1742-6596/1037/7/072041

Exploring a better turbine layout in vertically staggered wind farms

Mengqi Zhang[1,2], **Richard J.A.M. Stevens**[1]

[1] Physics of Fluids Group, Max Planck Center Twente for Complex Fluid Dynamics, J. M. Burgers Center for Fluid Dynamics, and MESA+ Research Institute, University of Twente, P.O. Box 217, 7500 AE Enschede, The Netherlands

[2] Department of Mechanical Engineering, National University of Singapore, 10 Kent Ridge Crescent, 119260, Singapore

E-mail: mpezmq@nus.edu.sg, r.j.a.m.stevens@utwente.nl

Abstract. Vertical staggering of wind turbines can lead to an increased power production in the entrance region of a wind farm because downstream turbines are consequently outside the wakes of preceding turbines. We perform large eddy simulations of different vertically staggered wind farm configurations for which we keep the average turbine hub height the same. We find that the turbine power output in the entrance region of the wind farm is significantly higher when the first turbine row is elevated than when the first turbine row is lowered. The reason is that this allows the first high turbine row to fully benefit from the strong winds at a high elevation. In the fully developed region of the wind farm the power production of the vertically staggered wind farms is similar to the power production of the corresponding reference aligned wind farm, while the normalized power fluctuations can be significantly higher than in the reference wind farm.

1. Introduction

In order to optimize the performance of large wind farms it is important to minimize wake effects. Many research efforts have focused on using horizontal staggering to improve wind farm performance [1]. However, the potential use of vertical staggering to improve the performance of wind farms is much less explored. So far, most studies on vertical staggering have used simple analytical wake models such as the Jensen model [2] in combination with various optimization methods [3] to study the effect of vertical staggering in optimizing the wind farm configuration [4–7].

However, reliable reference data for the effect of vertical staggering on wind farm performance from experiments [8,9] or high-fidelity numerical simulations [9,10], such as large eddy simulations (LES), are still very limited. We recently investigated the effect of vertical staggering using LES [11] and found that the power output in the entrance region of a wind farm can be significantly increased by vertically staggering the turbines compared to a reference case, where the turbines are vertically aligned. The benefit of vertical staggering is larger when the turbine spacing and turbine diameter are smaller. In addition, we found that the beneficial effect of vertical staggering diminishes downstream in the wind farm because the downward vertical kinetic energy flux, which transfers the energy from the atmospheric flow above the wind farm to the hub height plane, does not increase due to vertical staggering. We also found that the

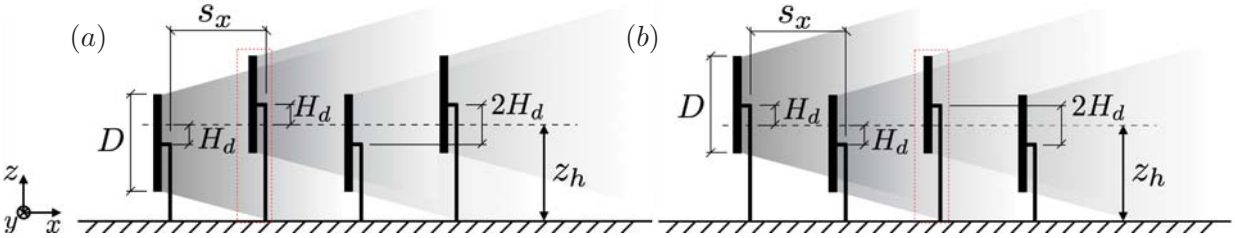

Figure 1. Sideview of the conceptual configuration of a vertically staggered wind farm with (a) odd turbine rows lowered and (b) odd turbine rows elevated. The grey patterns represent linearly expanding wakes behind the turbines. The dimensionless streamwise turbine spacing s_x is measured in terms of the turbine diameter D. The average turbine hub height is z_h and H_d measures the height difference with respect to z_h such that the hub height difference between consecutive rows is $2H_\mathrm{d}$. The red dashed boxes facilitate the discussion in figure 7.

Table 1. The columns from left to right indicated the case name, the turbine hub height z_h and diameter D, H_d (see figure 1), and $N_\mathrm{T,x}$ and $N_\mathrm{T,y}$, which indicate the number of turbines in streamwise and spanwise directions, respectively. The last two columns give the ratio of the power production of the turbines in the first and last four rows of the vertically staggered wind farms over the power production obtained in the corresponding reference aligned wind farm.

Cases	z_h (m)	D (m)	H_d (m)	$N_\mathrm{T,x}\times\ N_\mathrm{T,y}$	s_x	Power of first 4 rows	Power of last 4 rows
$A_\mathrm{reference}$	100	100	0	18×6	5.24	-	-
$A_\mathrm{odd\ lowered}$	100	100	40	18×6	5.24	1.122	1.010
$A_\mathrm{odd\ elevated}$	100	100	40	18×6	5.24	1.152	0.995
$B_\mathrm{reference}$	100	100	0	14×6	6.98	-	-
$B_\mathrm{odd\ lowered}$	100	100	40	14×6	6.98	1.050	0.955
$B_\mathrm{odd\ elevated}$	100	100	40	14×6	6.98	1.069	0.947
$C_\mathrm{reference}$	120	150	0	12×4	5.24	-	-
$C_\mathrm{odd\ lowered}$	120	150	30	12×4	5.24	1.038	1.000
$C_\mathrm{odd\ elevated}$	120	150	30	12×4	5.24	1.097	1.015
$D_\mathrm{reference}$	120	150	0	8×4	6.98	-	-
$D_\mathrm{odd\ lowered}$	120	150	30	8×4	6.98	1.035	1.016
$D_\mathrm{odd\ elevated}$	120	150	30	8×4	6.98	1.069	1.025

predictions from simple analytical models such as the Jensen model do not necessarily capture the performance of large vertically staggered wind farms well [11].

This necessitates the use of high-fidelity numerical simulation tools such as LES to study the flow dynamics in vertically staggered wind farm in order to increase our physical understanding and to generate reliable reference data for model development. Previously, we considered only one specific vertically staggered wind farm layout, that is a wind farm with shorter turbines in the odd rows and higher turbines in the even rows, see figure 1a [11]. Here we also consider another layout with higher turbines placed in odd rows and shorter ones in even rows, see figure 1b. We are interested in this configuration because of its potential to achieve higher power output in the entrance region of the wind farm. We compare the vertically staggered wind farms under consideration with a reference aligned wind farm in which all turbines have the same hub height, which matches the average hub height of the turbines in the vertically staggered wind farms. This allows us to assess the potential benefit of vertical staggering.

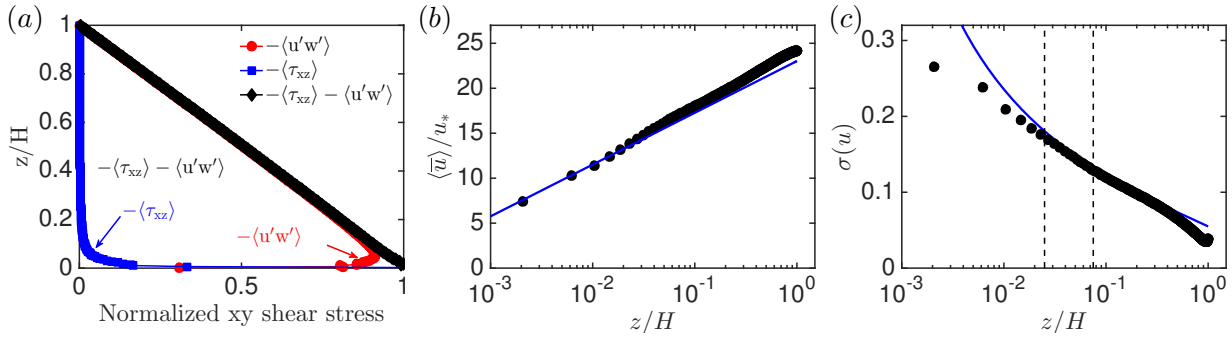

Figure 2. (a) Vertical profiles of the resolved stress ($-\langle u'w'\rangle$, circles) the normalized sub-grid scale stress ($-\langle\tau_{xz}\rangle$, squares) and the total stress ($-\langle u'w'\rangle - \langle\tau_{xz}\rangle$, diamonds). Vertical profile of the (b) mean and (c) turbulence intensity profiles compared to the theoretical predictions, see details in text.

2. Numerical method and simulation cases

In our simulations we consider finite size wind farms in a neutral atmospheric boundary layer and assume that the Coriolis force is negligible. We use a pseudo-spectral discretization in the horizontal directions and a central second order finite difference scheme in the vertical direction. The sub-grid scale dynamics are modeled by the Lagrangian averaged scale dependent dynamic model [12] and time integration is performed using a second order Adams-Bashforth scheme. We use the concurrent precursor inflow method [13] to generate the inflow conditions by feeding the wind farm simulation with fully developed turbulent boundary layer flow to accurately represent the characteristics of the incoming flow. Figure 2a confirms that the inflow condition has indeed reached the statistically stationary state and shows the resolved and sub-grid shear stresses in the atmospheric boundary layer. To reduce the effect of the location of the high and low velocity speed streaks we perform the simulations for a long time and very slowly shift the entire flow in the inflow generating domain in the spanwise direction to get well converged streak independent results. This method is tested in Ref. [14], and the benefits of such a method are discussed in more detail by Munters *et al.* [15]. Figure 2b shows that the inflow conditions generated with this method capture the logarithmic law for the mean $\langle\overline{u}\rangle/u_* = \kappa^{-1}\ln(z/z_{0,\mathrm{lo}})$, where $z_{0,\mathrm{lo}}$ is the roughness height at the ground and κ the von Kármán constant. Figure 2c shows the turbulence intensity profile $\sigma(u) = [\langle\overline{(u')^2}\rangle]^{1/2}/\langle\overline{u}\rangle$ for the inflow compared to the theoretical prediction, which is based on the logarithmic law for the mean and the variance, which reads $\langle\overline{(u')^2}\rangle/(u^*)^2 = B_1 - A_1\log(z/H)$, with $A_1 \approx 1.25$, $B_1 = 1.6$, and H the boundary layer height [14, 16].

The turbines are modeled using an actuator disk model, which has been shown to reasonably accurately capture wake profiles further downstream with a much lower computational cost [13,14,17–19] than an actuator line model [20,21]. The average power output of turbines is equal to the mechanical energy loss in the fluid, i.e. $P = -\langle FU_\mathrm{d}\rangle$ where $F = -\frac{1}{2}C'_\mathrm{T}\rho U_\mathrm{d}^2 A$ is the local force used in the actuator disk model with U_d being the disk averaged velocity, $A = \pi D^2/4$ the turbine rotor area, and $C'_\mathrm{T} = C_\mathrm{T}/(1-a)^2$, where a is the axial induction factor, see Refs. [18,22] for details. This simulation approach has been validated against wind tunnel measurements performed at EPFL [14], Delft [23], and the Horns Rev wind farm measurements [13].

The size of the wind farm domain is $2\pi H \times 0.5\pi H \times H$ in streamwise, spanwise, and vertical direction, respectively, which is discretized on a grid with $512 \times 128 \times 241$ computational nodes. This ensures that the large scale dynamics are captured and that the results are grid independent as is shown in, for example, Refs. [13,24,25]. In this study we consider cases with smaller turbines ($D_\mathrm{s} = 100$m and $z_\mathrm{h} = 100$m) and larger turbines ($D_\mathrm{l} = 150$m and $z_\mathrm{h} = 120$m), while setting $H = 2000$m and $z_{0,\mathrm{lo}}/H = 10^{-4}$. The bigger wind turbine is considered because of the recent

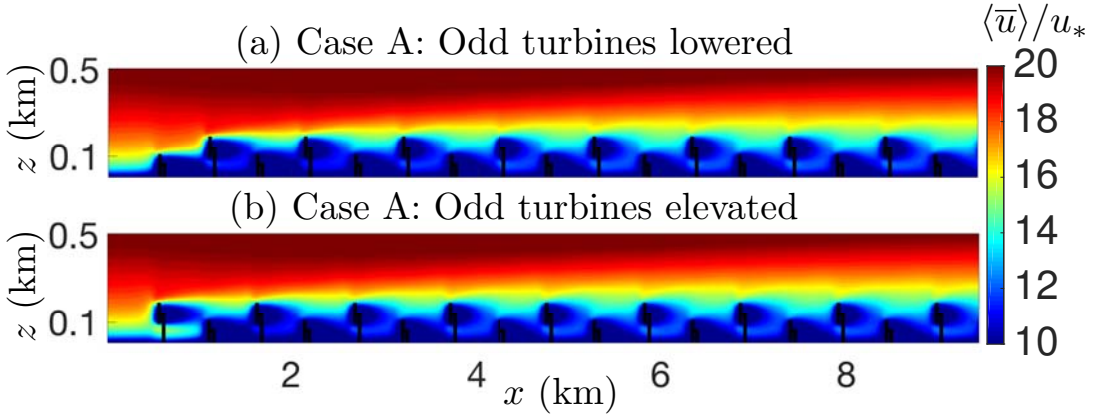

Figure 3. Time averaged streamwise velocity in the vertical cross section intersecting the turbines for case A, see table 1, with the (a) odd turbine lowered and (b) odd turbines elevated. The black vertical lines indicate the wind turbine positions.

development trend towards larger turbines [26]. The turbine distances are made dimensionless using either D_s or D_l. We keep the spanwise spacing $s_\mathrm{y} = 5.24$ fixed, and consider two different streamwise turbine spacings s_x, i.e. $s_\mathrm{x} = 5.24$ and $s_\mathrm{x} = 6.98$. For each of the corresponding four cases (labeled as cases A to D) we consider a reference aligned case and two vertically staggered cases, one in which the odd turbine rows are lowered and one in which the odd turbine rows are elevated. This allows us to study the effect of different vertical staggering configurations on the wind farm performance. The parameter H_d, see figure 1, indicates how much vertical staggering is applied. We ensure that the lowest part of all turbine rotors is at least 10 meters from the ground. A summary of the considered cases is shown in table 1.

3. Results

Figure 3 shows the time averaged streamwise velocity field in the two vertically staggered wind farms of case A and reveals that an internal boundary layer is formed at the start of the wind farm. In the entrance region of the wind farm there are pronounced differences due to the different vertical staggering configurations, however the flow field in the fully developed region looks very similar for both cases. To investigate the influence of the different vertical staggering configurations we show the row averaged turbine power outputs, normalized by the power output of a free standing turbine with hub height z_h, as function of downstream position for all cases in figure 4. This figure reveals that the average power production in the entrance region of the wind farm is higher when the odd turbine rows are elevated than when the even turbine rows are elevated. For both vertical staggered configurations we find that the power production in the fully developed region is comparable to the production obtained in the reference aligned wind farm [11].

In table 1 and figure 5 we substantiate these observations by comparing the power production of the vertically staggered wind farms with the corresponding reference aligned wind farms. Table 1 shows that elevating the odd turbine rows, and lowering the even turbine rows, leads to a significant increase in the power production of up to 15% compared to the reference aligned case for the first four turbine rows. The benefit compared to the reference case is much smaller, i.e. up to approximately 6%, when the even turbine rows are elevated and the odd turbine rows are lowered. The reason is that elevating the first turbine row ensures that these turbines can take full advantage of the undisturbed atmospheric flow at a higher altitude. Instead, when the second turbine row is elevated it will still be partially in the wake created by turbines on the first row, due to which this higher turbine row can take less advantage of the strong winds at higher

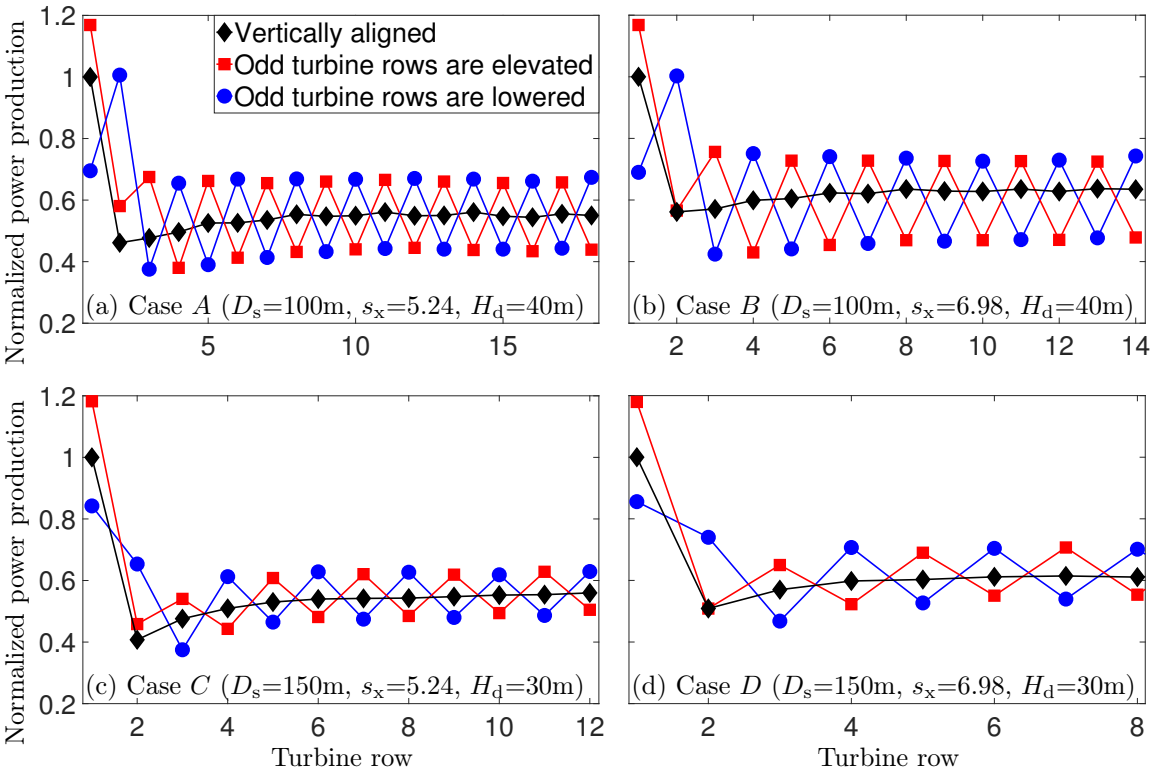

Figure 4. Normalized power production as function of the downstream position. Each panel shows the result for the reference aligned and the two vertically staggered wind farm configurations for one of the cases A to D, see table 1. The results are normalized by the power production of the first turbine row of the reference aligned wind farm.

elevation. Table 1 shows that the production in the fully developed region of the wind farm, here defined as the last 4 turbine rows considered in our simulations, in the vertically staggered wind farms is very close to the production obtained in the reference aligned wind farm. For case B we even see that the production in the fully developed region is about 5% lower in the vertically staggered wind farms than in the corresponding reference aligned case.

Figure 5 shows the relative cumulative production, which we define as the ratio of the cumulative production of the vertically staggered wind farm over the production in the reference aligned wind farm up to that downstream location, for the two vertical staggered wind farm configurations. The figure shows, in agreement with the results in table 1, that the largest benefit of vertical staggering is obtained in the entrance region of the wind farm. In fact, figure 5 reveals that the largest relative benefit of vertical staggering is expected for wind farms with two to four rows in downstream direction and further downstream the relative cumulative production converges slowly to unity as the production in the fully developed region is almost the same in the vertically staggered wind farm and the reference aligned wind farm. For case B, for which the production in the fully developed region is lower in the vertically staggered wind farms than in the reference aligned wind farm, the relative cumulative production eventually drops below unity.

To gain a better understanding of the performance in the fully developed region of the wind farm, we look into the vertical kinetic energy flux for different wind farm configurations. For large wind farms, this energy flux is the main reason the wind turbine wakes inside the wind farm recover and the kinetic energy of the flow at hub height is replenished [11, 18, 22, 27–30]. Figure 6a and b show the vertical profile of the spanwise averaged vertical kinetic energy

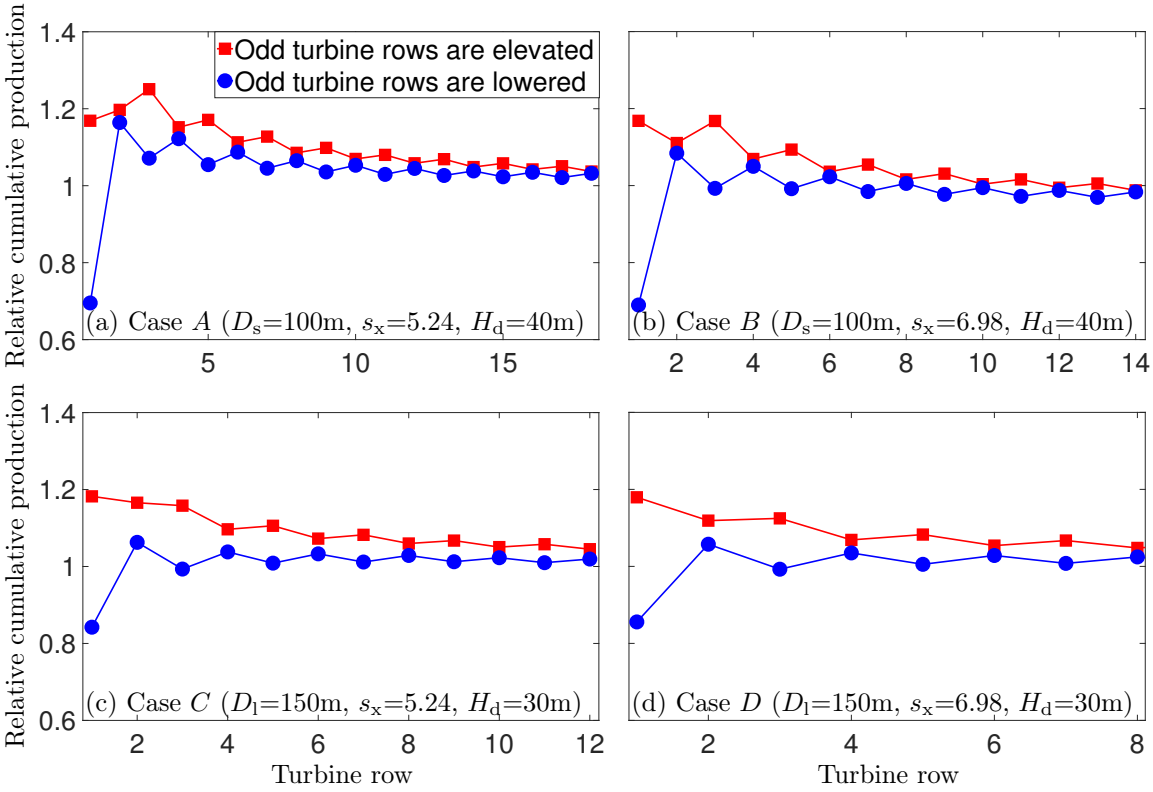

Figure 5. The relative cumulative power production, i.e. the ratio of the power production in the vertically staggered wind farms over the production of the reference aligned wind farm, as function of downstream position for cases A to D, see table 1.

flux $\langle\Phi\rangle = -\langle\overline{u}\rangle\langle\overline{u'w'}\rangle$, where u' and w' are the normalized streamwise and vertical velocity fluctuations, at several downstream locations in the wind farm. Comparing figure 6a and b reveals that the vertical kinetic energy flux profile becomes approximately independent of the wind farm configuration after row 6. A more intriguing result is presented in figure 6c and d where the spanwise averaged vertical kinetic energy flux at $z = 300$m as function of downstream position is shown for cases A ($s_x = 5.24$ and $D = 100$m) and B ($s_x = 6.98$ and $D = 100$m). For case A we observe that vertical staggering does not significantly change the vertical kinetic energy flux compared to the reference aligned case. This result is in agreement with the observation that for case A the production in the fully developed region is similar for the vertically staggered and reference aligned wind farm and the view that the production in the fully developed region is mainly determined by the vertical kinetic energy flux. For case B we observed that the production in the fully developed region is about 5% lower in the vertically staggered wind farms than in the corresponding reference aligned wind farm. In agreement with this figure 6d shows that for case B the vertical kinetic energy flux is slightly lower for the vertically staggered wind farms than for the corresponding reference aligned wind farm. A closer inspection of figure 4 reveals that the production of the short turbines is almost the same in case A and case B, even though the streamwise turbine spacing between consecutive turbine rows is significantly larger for case B. For the reference aligned wind farm and the higher turbines in the vertically staggered wind farms we see that this larger streamwise turbine spacing is reflected in a better turbine performance. We thus conclude that the lower power production in the fully developed region of the vertically staggered wind farms of case B is because the production of the short turbines lags behind.

In figure 7 we compare the streamwise velocity profiles for the different wind farm configurations of case A, see table 1, at different downstream locations. Figure 7c and d show

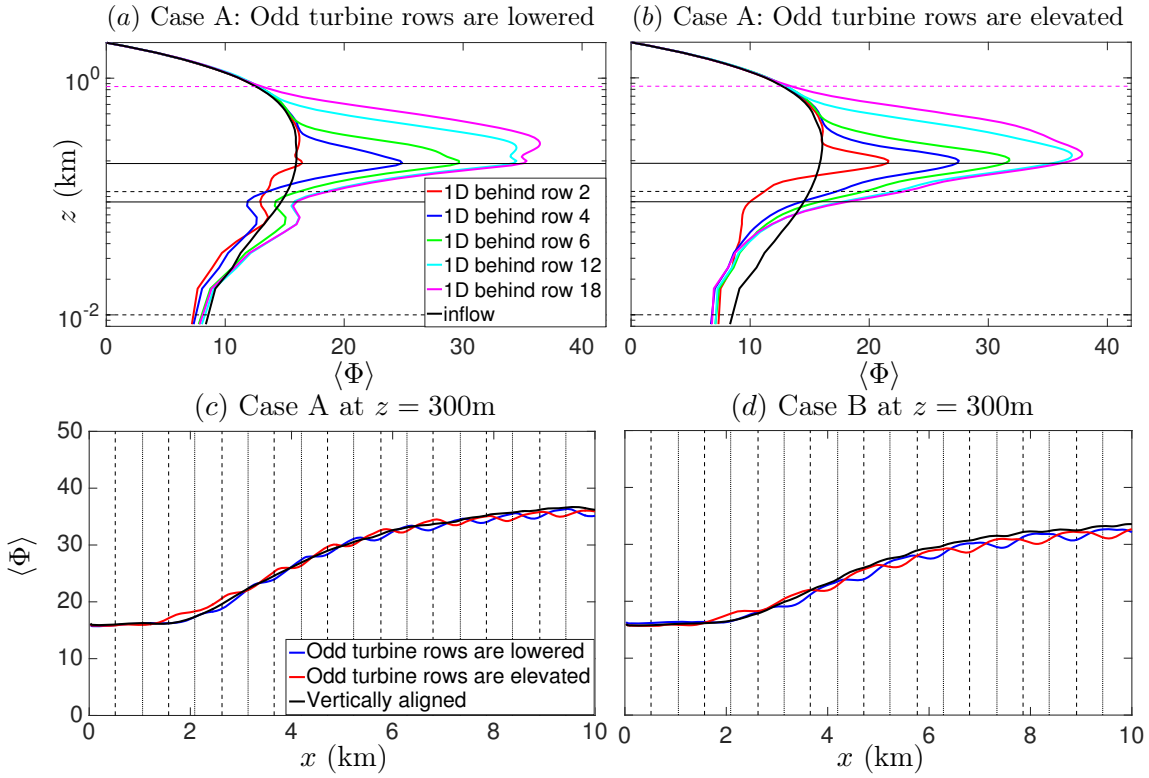

Figure 6. Vertical profile of the spanwise averaged vertical kinetic energy flux $\langle\Phi\rangle$ one turbine diameter downstream of the respective turbine rows for case A, see table 1, in which (a) the odd turbine are lowered and (b) the odd turbines are elevated. The horizontal dashed and solid lines indicate the top and bottom of the rotors of the shorter and higher turbines, respectively. The horizontal dashed magenta line indicates the internal boundary layer thickness $\delta = 850$m in the fully developed region on the wind farm. The development of the vertical kinetic energy flux $\langle\Phi\rangle$ as function of downstream position at $z = 300$m for case (c) A and (d) B, see table 1.

that in the fully developed region the velocity profiles in the two vertically staggered wind farm configurations are nearly identical, which is in agreement with our earlier conjuncture based on figure 3. Figure 7a and b show that there are some differences in the observed wake effects in the entrance region. Here we are specifically looking at the higher turbines in the 2$^{\text{nd}}$ and 3$^{\text{rd}}$ rows, see also the highlighted turbines in the sketch of figure 1. Figure 7 shows that the wake effects behind this high turbine is stronger for the case in which the odd turbine rows are elevated than for the configuration in which the odd turbine rows are lowered.

While the average power production is, in many cases, the first quantity of interest, it is also important to consider what effect the usage of vertical staggering could have on the unsteady turbulence loading the turbines in the wind farm may experience. However, as our simulations are performed using an actuator disk model we do not have access to these loads. To gain some understanding of the effect vertical staggering may have on the turbine loads, we show in figure 8 the standard deviation of the power fluctuations normalized by the average power production for the wind farms of case A and C. For the first turbine row we see that the normalized power fluctuations are higher for the vertically staggered wind farm in which the odd turbine rows are lowered than in the vertically staggered wind farm in which the odd turbines are elevated. This observation is in agreement with the turbulence intensity profile of the incoming flow, see figure 2b. Figure 8a shows that after the third row the power fluctuations are significantly higher in the vertically staggered wind farms of case A than in the corresponding reference aligned wind

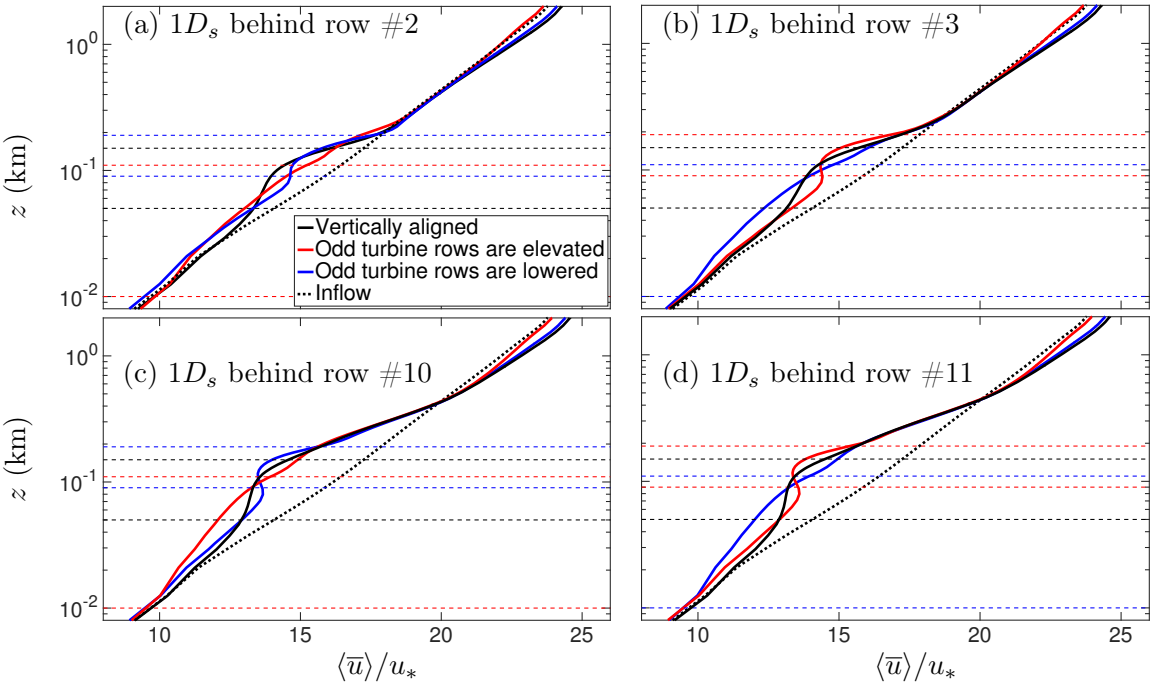

Figure 7. Vertical profile of the horizontally averaged streamwise velocity $1D_s$ downstream of the indicated turbine row for case A, see table 1. The dash dotted line indicates the inflow condition. The horizontal dashed lines indicate the top and bottom of the rotors of the wind turbines in the preceding row.

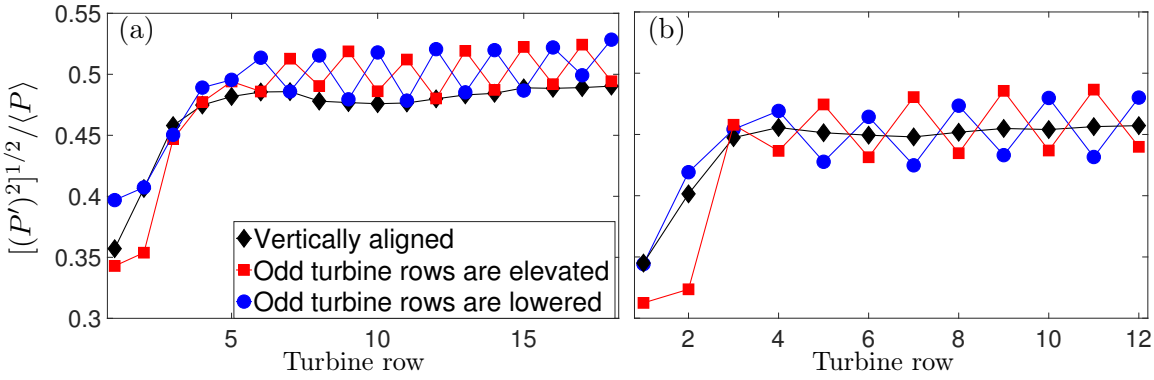

Figure 8. Normalized power fluctuations $[(P')^2]^{1/2}/\langle P\rangle$ per row for (a) case A and (c) case C, see table 1, as function of downstream position.

farm. This suggests that higher turbine loadings could be higher in such vertically staggered wind farms than in the reference aligned wind farm. This increase in the power fluctuations is less pronounced for case C. However, we note that for case C the relative vertical staggering is much more limited, which is reflected in the lower row to row power variation in these vertically staggered wind farms, see figure 4c.

4. Conclusions

We used LES to study the effect of different vertical staggering configurations in large wind farms. We compared the performance of a reference aligned wind farm with two vertically staggered wind farm configurations, a configuration in which the odd turbine rows are elevated and the

even rows are lowered compared to a reference wind farm, and a configuration in which the odd turbine rows are lowered and the even rows are elevated. We find that the vertically staggered wind farm in which the odd turbine rows are elevated has the highest power production because the high turbines in the first rows can optimally benefit from the strong undisturbed winds at higher elevations. Our results also show that the increase in the power production in the entrance region of the wind farm due to vertical staggering is higher when the streamwise turbine spacing and the turbine rotor diameter are smaller. In the fully developed region of the wind farm, vertical staggering does not increase the power production compared to the reference aligned wind farm. For one case we even find a reduction in the power production in the fully developed region. The reason is that the vertical kinetic energy flux, which brings high velocity wind from above the wind farm to the hub-height plane, does not seem to be influenced much by vertically staggering [11]. Additionally, due to the slow wake recovery close to the ground, the power production of the shorter turbine rows can be significantly impacted, which can lead to a lower overall production in the fully developed region compared to the reference aligned case.

Here we showed that vertical staggering can increase the power production in the entrance region of a wind farm. However, we note that the potential use of vertical staggering should be carefully considered as this may have implications for the wind turbine manufacturer, requiring different designs for turbines of various sizes. In addition, as we show that vertical staggering can lead to a significant increase in the normalized power fluctuations for the turbines, more detailed simulation studies are required to carefully assess the effect of vertical staggering on the unsteady turbulence loading the turbines may experience in vertically staggered wind farms. On the other hand, in order to optimize the vertical staggering layout in the entrance region of wind farms, it is also necessary to test (and potentially further develop) computationally less demanding simulation tools such as RANS models to capture the effect of vertical staggering.

Acknowledgements
This work is part of the Shell-NWO/FOM-initiative Computational sciences for energy research of Shell and Chemical Sciences, Earth and Live Sciences, Physical Sciences, FOM and STW and an STW VIDI grant (No. 14868). This work was carried out on the national e-infrastructure of SURFsara, a subsidiary of SURF cooperation, the collaborative ICT organization for Dutch education and research.

References

[1] R. J. A. M. Stevens and C. Meneveau. Flow structure and turbulence in wind farms. *Annual Review of Fluid Mechanics*, 49(1):311–339, 2017.
[2] N. O. Jensen. A note on wind generator interaction. (Risø-M; No. 2411). Technical report, 1983.
[3] G. M. J. Herbert, S. Iniyan, and D. Amutha. A review of technical issues on the development of windfarms. *Renewable and Sustainable Energy Reviews*, 32:619–641, 2014.
[4] Y. Chen, H. Li, K. Jin, and Q. Song. Wind farm layout optimization using genetic algorithm with different hub height wind turbines. *Energy Conversion and Management*, 70:56 – 65, 2013.
[5] K. Chen, M.X. Song, X. Zhang, and S.F. Wang. Wind turbine layout optimization with multiple hub height wind turbines using greedy algorithm. *Renewable Energy*, 96, Part A:676 – 686, 2016.
[6] B. DuPont, J. Cagan, and P. Moriarty. An advanced modeling system for optimization of wind farm layout and wind turbine sizing using a multi-level extended pattern search algorithm. *Energy*, 106:802 – 814, 2016.
[7] A. Vasel-Be-Hagh and C. L. Archer. Wind farm hub height optimization. *Applied Energy*, 195:905 – 921, 2017.
[8] L. P. Chamorro, N. Tobin, R. E. A. Arndt, and F. Sotiropoulos. Variable-sized wind turbines are a possibility for wind farm optimization. *Wind Energy*, 17:1483–1494, 2014.
[9] S. Xie, C. L. Archer, N. Ghaisas, and C. Meneveau. Benefits of collocating vertical-axis and horizontal-axis wind turbines in large wind farms. *Wind Energy*, 20(1):45–62, 2017.
[10] L. Wang, A. C.C. Tan, M. Cholette, and Y. Gu. Comparison of the effectiveness of analytical wake models

for wind farm with constant and variable hub heights. *Energy Conversion and Management*, 124:189 – 202, 2016.

[11] M. Zhang, M. Arendshorst, and R. J. A. M. Stevens. Large eddy simulations of the effect of vertical staggering in extended wind farms. *submitted to Wind Energy*, 2018.

[12] E. Bou-Zeid, C. Meneveau, and M. B. Parlange. A scale-dependent Lagrangian dynamic model for large eddy simulation of complex turbulent flows. *Physics of Fluids*, 17:025105, 2005.

[13] R. J. A. M. Stevens, J. Graham, and C. Meneveau. A concurrent precursor inflow method for Large Eddy Simulations and applications to finite length wind farms. *Renewable Energy*, 68:46–50, 2014.

[14] R. J. A. M. Stevens, Luis A. Martínez-Tossas, and Charles Meneveau. Comparison of wind farm large eddy simulations using actuator disk and actuator line models with wind tunnel experiments. *Renewable Energy*, 116:470 – 478, 2018.

[15] W. Munters, C. Meneveau, and J. Meyers. Shifted periodic boundary conditions for simulations of wall-bounded turbulent flows. *Physics of Fluids*, 28:025112, 2016.

[16] R. J. A. M. Stevens, M. Wilczek, and C. Meneveau. Large eddy simulation study of the logarithmic law for high-order moments in turbulent boundary layers. *J. Fluid Mech.*, 757:888–907, 2014.

[17] A. Jimenez, A. Crespo, E. Migoya, and J. Garcia. Advances in large-eddy simulation of a wind turbine wake. *Journal of Physics: Conference Series*, 75(1), 2007. 012041.

[18] M. Calaf, C. Meneveau, and J. Meyers. Large eddy simulation study of fully developed wind-turbine array boundary layers. *Physics of Fluids*, 22(1), 2010. 015110.

[19] M. Calaf, M. B. Parlange, and C. Meneveau. Large eddy simulation study of scalar transport in fully developed wind-turbine array boundary layers. *Physics of Fluids*, 23(12):126603, 2011.

[20] N. Troldborg, J. N. Sørensen, and Robert Mikkelsen. Numerical simulations of wake characteristics of a wind turbine in uniform inflow. *Wind Energy*, 13:86–99, 2010.

[21] N. Troldborg, G. C. Larsen, H. A. Madsen, K. S. Hansen, J. N. Sørensen, and R. Mikkelsen. Numerical simulations of wake interaction between two wind turbines at various inflow conditions. *Wind Energy*, 14:859–876, 2011.

[22] R. J. A. M. Stevens, D. F. Gayme, and C. Meneveau. Large Eddy Simulation studies of the effects of alignment and wind farm length. *Journal Renewable and Sustainable Energy*, 6:023105, 2014.

[23] L. E. M. Lignarolo, D. Mehta, R. J. A. M. Stevens, A. E. Yilmaz, G. van Kuik, S. J. Andersen, C. Meneveau, C. J. Simão Ferreira, D. Ragni, J. Meyers, G. J. W. van Bussel, and J. Holierhoek. Validation of four LES and a vortex model against stereo-PIV measurements in the near wake of an actuator disc and a wind turbine. *Renewable Energy*, 94:510–523, 2016.

[24] Y.-T. Wu and F. Porté-Agel. Large-eddy simulation of wind-turbine wakes: Evaluation of turbine parametrisations. *Boundary-Layer Meteorology*, 138(3):345–366, 2011.

[25] Y.-T. Wu and F. Porté-Agel. Simulation of turbulent flow inside and above wind farms: Model validation and layout effects. *Boundary-Layer Meteorology*, 146(2):181–205, 2013.

[26] G. A. M. van Kuik, J. Peinke, R. Nijssen, D. Lekou, J. Mann, J. N. Sørensen, C. Ferreira, J. W. van Wingerden, D. Schlipf, P. Gebraad, H. Polinder, A. Abrahamsen, G. J. W. van Bussel, J. D. Sørensen, P. Tavner, C. L. Bottasso, M. Muskulus, D. Matha, H. J. Lindeboom, S. Degraer, O. Kramer, S. Lehnhoff, M. Sonnenschein, P. E. Sørensen, R. W. Künneke, P. E. Morthorst, and K. Skytte. Long-term research challenges in wind energy - a research agenda by the European Academy of Wind Energy. *Wind Energy Science*, 1:1–39, 2016.

[27] R. B. Cal, J. Lebrón, L. Castillo, H. Suk Kang, and C. Meneveau. Experimental study of the horizontally averaged flow structure in a model wind-turbine array boundary layer. *Journal Renewable and Sustainable Energy*, 2(1), 2010. 013106.

[28] C. VerHulst and C. Meneveau. Large eddy simulation study of the kinetic energy entrainment by energetic turbulent flow structures in large wind farms. *Physics of Fluids*, 26:025113, 2014.

[29] R. J. A. M. Stevens, D. F. Gayme, and C. Meneveau. Effects of turbine spacing on the power output of extended wind-farms. *Wind Energy*, 19:359–370, 2016.

[30] D. Allaerts and J. Meyers. Gravity waves and wind-farm efficiency in neutral and stable conditions. *Boundary-Layer Meteorology*, 166(2):269–299, 2018.